Research Square

Preprints are preliminary reports that have not undergone peer review.
They should not be considered conclusive, used to inform clinical practice,
or referenced by the media as validated information.

Structural Basis of Transcriptional Coactivator PC4 Binding to a Platinum Crosslinked Double-Stranded Oligonucleotide

Fuyi Wang

fuyi.wang@iccas.ac.cn

Institute of Chemistry, Chinese Academy of Sciences https://orcid.org/0000-0003-0962-1260

yuanyuan Wang

Min Zang

Nanjing Univeristy

Zhifeng Du

Beijing National Laboratory for Molecular Sciences, CAS Key Laboratory of Analytical Chemistry for Living Biosystems, Institute of Chemistry

Wei Zheng

Beijing National Laboratory for Molecular Sciences, CAS Key Laboratory of Analytical Chemistry for Living Biosystems, Institute of Chemistry

Juan Qiao

Beijing National Laboratory for Molecular Sciences, CAS Key Laboratory of Analytical Chemistry for Living Biosystems, Institute of Chemistry

Kui Wu

School of Chemistry and Chemical Engineering, Wuhan University of Science and Technology

Qun Luo

Institute of Chemistry, Chinese Academy of Sciences https://orcid.org/0000-0002-5186-3880

Li Qi

Institute of Chemistry, Chinese Academy of Sciences

Yao Zhao

Institute of Chemistry, Chinese Academy of Sciences https://orcid.org/0000-0003-0613-8708

Hao Dong

Nanjing University https://orcid.org/0000-0001-7280-7506

Article

Keywords:

Posted Date: February 27th, 2026

DOI: https://doi.org/10.21203/rs.3.rs-8574332/v1

License: This work is licensed under a Creative Commons Attribution 4.0 International License.
Read Full License

Additional Declarations: There is **NO** Competing Interest.

Abstract

We previously discovered that human nuclear cofactor PC4 selectively binds to a double-stranded oligodeoxynucleotide (dsODN) crosslinked by a *trans*-platinum anticancer complex, *trans*-[$PtCl_2(NH_3)$(thiazole)] (*trans*-PtTz), which was further demonstrated to reduce its cytotoxicity by mediating DNA repair, though the molecular mechanism was unclear. In this work, we developed an amide hydrogen/deuterium exchange mass spectrometry (HDX-MS) coupled to online peptic digestion to dissect interaction interface and binding sites between PC4 and a *trans*-PtTz crosslinked 15-mer dsODN (*trans*-PtTz-**III**). Using online HDX-MS, we identified a 1:1 binding stoichiometry and key involvement of the β3–β5 sheets (K80–Q109) in recognition. Molecular dynamic simulations suggest a 2:2 binding mode and the C-terminal helices slightly loosen, with Arg86 being critical for the recognition and interaction between PC4 and *trans*-PtTz-**III**. More importantly, site-directed mutation of Arg86 weakened the binding of PC4 to *trans*-PtTz-**III** in *vitro* and promoted the cytotoxicity of *trans*-PtTz against A549 cells. This work profiles the detailed interaction mechanism of PC4 with *trans*-PtTz damaged dsODN, and provides a new paradigm for the further research of the cellular response to platinum induced DNA damage.

Introduction

Human nuclear protein positive cofactor 4 (PC4) is an abundant multifunctional nuclear protein that plays important roles in various cellular processes such as transcription, DNA repair, replication, chromatin organization and cell cycle progression.[1−7] Usually, PC4 tends to form a homodimer, giving two DNA binding interfaces, so as to accommodate single-stranded DNA (ssDNA)[8−10] at DNA damage sites and recruit various proteins to exert their corresponding functions. PC4 might halt transcription by recognizing and stabilizing unpaired double-stranded DNA (dsDNA), ssDNA and/or DNA ends.[11,12] The common DNA repair intermediates or structures generated at DNA damage sites may also be recognized by PC4 to enable detection and repair of these lesions by introducing other DNA damage repair factors.[8,13,14] PC4 has also been reported to activate double-strand break repair by stimulating the joining of non-complementary DNA ends.[15] These indicate that PC4 plays an important role in the early response to DNA damage by recognizing ssDNA.[16]

DNA encodes genetic information and has long been considered as a preferential target for cancer chemotherapeutic agents.[12] The coordination of the widely used anticancer drug, cisplatin, to purine bases mainly forms 1,2-intrastrand crosslinks to distort DNA conformation by unwinding and bending the helix.[17] Such unique and severe lesions in DNA halt the normal transcription[18] and can be specially recognized by high mobility group (HMG) domain proteins, particularly HMGB1, which in turn impedes the repair of damaged sites and leads to apoptosis of cancer cells.[19]

On the contrary, as the inactive stereoisomer of cisplatin, transplatin (*trans*-diamminedichloroplatinum), mainly forms monofunctional and 1,3-GXG intrastrand crosslinking adducts.[20] The interactions of

cellular proteins with *trans*-platinum complex damaged DNA is still an open question. Besides, despite the analog of transplatin, *trans*-[$PtCl_2(NH_3)$(thiazole)] (*Trans*-PtTz) shares the same geometry as transplatin, it has shown significant cytotoxicity, even towards cisplatin-resistant cancer cell lines.[21] *Trans*-PtTz was shown to form monofunctional, 1,3-GXG intrastrand crosslinked and 1,2-GG interstrand crosslinked DNA adducts nearly in equal amount, and it was believed that the overall drug cytotoxicity of *trans*-PtTz could be the sum of the contributions of each of these adducts.[22] Therefore, it is important to investigate the roles of DNA adducts formed by *trans*-PtTz, especially the recognition and interactions of these different adducts with cellular proteins, which is significant for better understanding of the mechanisms of action of various *trans*-platinum complexes and improve the cytotoxicity of transplatinum complexes.

Our group has previously developed a strategy combining nanoparticle-based DNA affinity probes and MS-based quantitative proteomics, enabling us to discover that PC4 selectively recognize 1,3-GTG intrastrand crosslinked DNA by *trans*-PtTz.[23] Later, we revealed that the downregulation or silencing by siRNA of PC4 enhanced cytotoxicity of *trans*-PtTz against human HeLa ovarian cancer cells, suggesting that PC4 mediates the repair of *trans*-PtTz damaged DNA, which was evidenced by the increased accumulation of DNA-bound Pt in the cells.[24] However, the structural basis of this unique recognition and interaction remain unclear.

Hydrogen/deuterium exchange mass spectrometry (HDX-MS) has emerged as a rapid and sensitive approach for characterization of conformational changes of proteins following ligand binding.[25,26] The exchange rates between backbone amide hydrogens and deuterium of D_2O can be examined by MS so as to monitor the changes of the local environment around proteins, and the structural and dynamic aspects of the proteins in solution.[27] The binding interfaces upon the formation of protein-ligands complexes can be revealed by detecting changes in local deuterium uptake from digestion of deuterated proteins.[28,29] By comparing the difference of exchanged H/D numbers in different states, the interaction information with various molecules including nucleic acids on the protein surface can be obtained.[30] Unlike X-ray crystallography requiring crystallization of protein-DNA complexes and NMR needing large amount of purified samples, mass spectrometry has high resolution and sensitivity, so only a small amount of sample in solution (< 1 mg/experiment at low mM concentration) is enough to obtain useful information, even for large proteins and ligands like DNA.[31]

To this end, in this work, we use HDX-MS to characterize the interaction interface a *trans*-PtTz 1,3-GTG intrastrand crosslinked oligodeoxynucelotide (ODN) with PC4. To achieve this goal, a 1,3-intrastrand crosslinked 15-mer dsODN in which *trans*-PtTz binds to a -GTG- moiety was constructed. Then, the detailed binding conformation of the platinated ODN with a recombinant PC, in particular the key amino acid residues of PC4 at the binding interface were revealed by HDX-MS combined with a house-made online pepsin digestion device. Further, molecular dynamics simulation was employed to evaluate the binding affinity of the key amino acids between PC4 and the *trans*-PtTz crosslinked dsODN and the level of conformational change. Finally, site-directed amino acid mutation at Arg86 of recombinant PC4 and

intracellular PC4 in A549 human non-small-cell lung cancer cells were performed to interpret the experimentally determined recognition details, showing that Arg86 is the key site dominating the interaction of PC4 with *trans*-PtTz damaged DNA, which in turn regulate the cytotoxicity of *trans*-PtTz against A549 cells.

Results

Construction of the platinum crosslinked ODN complex

To construct a model dsODN containing 1,3-GTG intrastrand crosslink by *trans*-PtTz (Fig. 1a), we synthesized an oligodeoxyribonucleotide (ODN) duplex[23] which contains a pyrimidine-rich top strand with only two G bases (Fig. 1b) separated by one T in between. The top strand **I** was modified by *trans*-PtTz so that it contained a single 1,3-GTG intrastrand crosslink. At the given reaction condition with the molar ratio of Pt/**I** = 0.8, the 1,3-GTG intrastrand crosslinked ODN **I** by *trans*-PtTz was the main adduct which was confirmed by the HPLC analysis. In the chromatogram of the reaction mixture, only one new peak besides the free strand **I** was observed (Supplementary Fig. S1a). This product fraction was collected and characterized by ESI-MS under negative ion mode where the observed (obs.) *m/z* 1195.4187 (*z*=4) and *m/z* 1594.2341 (*z*=3) were assignable to the *trans*-PtTz 1,3-GTG intrastrand crosslinked strand **I**, corresponding to the calculated (calc.) *m/z* 1195.4219 and *m/z* 1594.2344, respectively (Supplementary Fig. S1b). Then strand **I** with the 1,3-intrastrand crosslink of *trans*-PtTz was subsequently annealed with its complementary strand **II** in 100 mM $NaClO_4$ solution to give rise to the 1,3-intrastrand *trans*-PtTz crosslinked duplex ODN (1,3-*trans*-PtTz-**III**, Fig. 1b) for further use.

Global H/D exchange of PC4 binding to 1,3-*trans*-PtTz-III

The global amide H/D exchange (HDX) of recombinant PC4 protein with or without ligation with 1,3-*trans*-PtTz-**III** was firstly examined. To minimize back-exchange of amide hydrogens, a fast LC gradient (6 min) was applied to elute the deuterated protein. At low pH (ca. 2.5) required for quenching HDX of amide hydrogens, all carboxylic groups ($pK_a \approx 4.6$) are protonated, making the proteins positively charged. While on the other hand, the oligodeoxynucleotides still have negative net charges due to the presence of backbone phosphate, which may result in the formation of stable protein/DNA precipitates, and interfere with the HPLC separation and MS analysis of the proteins. Therefore, protamine sulfate was added to avoid co-precipitation of proteins and ODNs.[32] The global deuterium uptake ratio was calculated by Equation 1 shown in Experimental Section and the corresponding kinetic plots versus time of HDX at 293 K for apo-PC4 (free intact protein) and holo-PC4 (1,3-*trans*-PtTz-**III**-PC4 complex) were obtained by analyzing the corresponding mass spectra (Supplementary Fig. S2), and shown in Fig. 1c.

The apo-PC4 approached the maximum deuteration in ca. 20 min of HDX at 293 K (Fig. 1c) and an average of 67 backbone amide hydrogens of PC4 were exchanged with deuterium, as indicated by the maximum mass shift of 67 Da. This number was much less than the 126 total amide hydrogens available for deuterium exchange, and the ratio of deuteration (53.2%) was less than the percent of D_2O

used in the experiments (90%). One of the possible reasons is the substantial back exchange of amide hydrogens during HPLC separation. Another possible reason for the low deuterium ratio of intact PC4 is that some amide hydrogens locating deeply inside the steric conformation of the protein are not solvent accessible. Besides, the formation of homodimer through the contacting of two symmetrical α-helixes in opposite direction as revealed by crystallography characterization [8,9] may also hamper the deuterium of PC4.

Upon binding with 1,3-*trans*-PtTz-**III**, the number of the deuterium uptake of the PC4 incubated in 90% D_2O for 1 min was only 55, which was substantially less than that of apo-PC4 (Fig. 1c). With the increase of incubation time, the number of exchanged deuterium of holo-PC4 quickly increased to 63 in about 10 min, but still lower than that of apo-PC4. These results suggests that the binding of 1,3-*trans*-PtTz-**III** to PC4 significantly shielded the backbone amide hydrogens from exchanging with deuterium in solution. The difference in global deuterium uptake implied the strong and specific binding of PC4 with the *trans*-PtTz crosslinked ODN. The HDX rate as pseudo-first order reactions of the apo-PC4 and holo-PC4 were calculated to be $(4.0 \pm 0.8) \times 10^{-2}$ and $(1.0 \pm 0.1) \times 10^{-3}$, respectively, based on the kinetic curves shown in Fig. 1c.

Fig. 1 a, Chemical structure of *trans*-[$PtCl_2(NH_3)$(thiazole)] (*trans*-PtTz). **b**, the sequences of single strand ODN **I**, **II** and double stranded **III** used in this work. The guanine bases in bold in strand **I** refer to the 1,3-platination sites. **c**, Kinetic curves for the global deuterium uptake of native PC4 (square) and ligated PC4 with 1,3-*trans*-PtTz-**III** (triangle). **d**, The global deuterium uptake of PC4 as a function of molar ratio of 1,3-*trans*-PtTz-**III** to PC4. The hydrogen/deuterium exchange time was 60 min at 293 K, and the deuterium incorporation numbers are the means of three independent measurements. **e**, Schematic set up of the online digestion and peptide separation device in this work. Green arrows indicate the direction of samples and mobile phases. Valve A is in position “inject” (solid lines) and can be switched to “load” (dashed lines). Valve B is in position displayed in solid lines for sample loading in trap column and can be shifted to position in dashed lines for HPLC analysis.

The binding stoichiometry was next determined by titrating recombinant PC4 (100 μM) with various concentrations of 1,3-*trans*-PtTz-**III** (from 0 to 300 μM) at pH 7.4. After quenching the HDX with 20% FA, the deuteride protein was introduced to the HPLC and mass spectrometer to determine the global deuterium uptake under different reaction molar ratios. The global deuterium uptake of the protein was plotted as the function of the molar ratio of 1,3-*trans*-PtTz-**III** to PC4 (Fig. 1d). With the increased concentration of 1,3-*trans*-PtTz-**III**, the global deuterium uptake of PC4 sharply decreased at the beginning and then reached an equilibrium when the number of the deuterium uptake of PC4 decreased to 62. The maximum number of deuterium uptake for holo-PC4 in the titration experiment was similar to that for global deuterium uptake described above. The turning point of the plot indicated that one PC4 molecule can bind to only one platinated ODN molecule (1,3-*trans*-PtTz-**III**).

Local H/D exchange of PC4 binding to 1,3-*trans*-PtTz-III

The difference between the global HDX of apo-PC4 and holo-PC4 drove us to explore further their details when binding to 1,3-*trans*-PtTz-**III** by local HDX experiments. To efficiently and accurately determine the deuterium uptake at peptide level so as to dissect the interaction interface of PC4 and *trans*-PtTz-platinated dsODN, an online pepsin digestion column was constructed according to a previously reported procedure[33] and applied into the HPLC system, as depicted in Fig. 1e. Pepsin derived from pepsinogen immobilized in the HPLC column functions under acidic condition compatible to the pH of the quenching solution after HDX (pH = 2 – 3) and tends to cleave at various positions to give small peptides (3 – 30 amino acids) and. Firstly, apo-PC4 was introduced as a model to evaluate the efficiency of the online pepsin digestion column coupled to a HPLC-ESI-MS system. Totally 20 peptides were identified, covering 86.6% of the sequence of PC4 (Table 1 and Supplementary Fig. S3). The identified peptides were assignable with sufficient signal-to-noise ratios with the mass error < ±60 ppm. Peptides Pep1 – Pep7 are located at the two serine-rich loops that belong to the flexible N-terminal of PC4. Peptides Pep8 – Pep13 cover the five β-sheet regions of PC4. Pep14 – Pep20 belong to the only α-helix region which, in combination with Pep13 from the β-sheet region, is important for PC4 dimerization.[8,9] Although there was some overlap among the identified peptides, the potential DNA binding domain of PC4 on the β-sheets[8,9,34] were successfully recognized, which provides adequate structural information for localizing the interaction interface between PC4 and 1,3-*trans*-PtTz-**III**.

Table 1. Identified peptides designated as Pep 1 – 20 of apo-PC4 by online pepsin digestion coupled with HPLC-ESI-MS.

Peptide	Sequence	Observed (*m/z*)	Calculated (*m/z*)	Error (ppm)
Pep1	M_1PKSKE_6	360.1911^{2+}	360.1915^{2+}	-1.11
Pep2	$M_1PKSKELVS_9$	509.7826^{2+}	509.7837^{2+}	-2.16
Pep3	$M_1PKSKELVSSSSSGSDSD_{18}$	914.4224^{2+}	914.4175^{2+}	5.36
Pep4	$P_{36}VKKQKTGETS_{46}$	601.8619^{2+}	601.8438^{2+}	30.1
Pep5	$T_{42}GETSRALSSSKQS_{55}$	719.8495^{2+}	719.8594^{2+}	-13.8
Pep6	$L_{49}SSSKQSSSSRDDNM_{63}$	814.8641^{2+}	814.8594^{2+}	5.77
Pep7	$S_{52}KQSSSSRDD_{61}$	548.7311^{2+}	548.7500^{2+}	-34.4
Pep8	$R_{59}DDNMFQIGKMRYVSVRDFKG_{79}$	854.7437^{3+}	854.7578^{3+}	-16.5
Pep9	$F_{64}QIGKMRY_{71}$	521.7778^{2+}	521.7813^{2+}	-6.71
Pep10	$I_{66}GKMRYV_{72}$	433.7264^{2+}	433.7495^{2+}	-53.3
Pep11	$R_{70}YVSVRDFKGKVLID_{84}$	559.0115^{3+}	559.0116^{3+}	-0.18
Pep12	$K_{80}VLIDIREYWMDPEGE_{95}$	996.9883^{2+}	996.9904^{2+}	-2.11
Pep13	$I_{85}REYWMDPEGEMKPGRKGISLNPEQ_{109}$	987.4794^{3+}	987.4844^{3+}	-5.06
Pep14	$N_{106}PEQWSQLKEQISDIDD_{122}$	1022.9307^{2+}	1022.9766^{2+}	-44.9
Pep15	$W_{110}SQL_{113}$	553.2738^{+}	553.2734^{+}	0.72
Pep16	$W_{110}SQLKEQISDIDD_{122}$	788.8779^{2+}	788.8750^{2+}	3.68
Pep17	$Q_{112}LKEQISDIDDAVR_{125}$	815.4430^{2+}	815.4297^{2+}	16.3
Pep18	$K_{114}EQISDIDD_{122}$	1062.4957^{+}	1062.4922^{+}	3.48
Pep19	$I_{120}DDAVRKL_{127}$	465.2752^{2+}	465.2734^{2+}	3.87
Pep20	$V_{124}RKL_{127}$	515.3652^{+}	515.3664^{+}	-2.33

The deuterium uptake of individual peptic peptide of apo-PC4 and holo-PC4 were then measured subjected to a 120 min continuous HDX at 293 K and the deuterium uptake ratio was calculated by Equation 1. The time dependent change in deuterium exchange levels and the ESI mass spectra at 1 and 120 min, respectively, of representative peptides, Pep6 (L49 – M63), Pep13 (I85 – Q109) and Pep16 (W110 – D122), derived from apo- and holo-PC4, are shown in Fig. 2a – f. The analogous plots of the rest

of the peptides are depicted in Supplementary Fig. S4 – S12 in the Supplementary Materials. The heat map in Fig. 2g shows the change of deuteration ratio for all the peptides identified by MS. These results indicate that over 120 min of HDX, there were no pronounced change in the deuteration ratio of peptic peptides Pep1 – Pep4, Pep9 – Pep11 and Pep19 – Pep20, which derived from the loop (M1 – K41), β1 – β2 sheets (F64 – D84) and C-terminal α-helix (I120 – L127), respectively, between apo- and holo-PC4. However, for peptide Pep5 (T42 – S55), Pep6 (L49 – M63) and Pep7 (S52 – D61), upon binding to 1,3-*trans*-PtTz-**III**, their maximum deuterium uptake significantly decreased compared to these in apo-PC4. This suggests that the interaction between PC4 and *trans*-PtTz-**III** prevented the HDX of the backbone amide hydrogens in these peptides. Considering that Pep1 – Pep4 (M1 – S46) were almost not affected in the ratio of deuterium uptake due to the platinated ODN binding, the residues R47 to M63 belonging to the flexible serine-rich loop in the N-terminal (Supplementary Fig. S3) must play an important role in the recognition and interaction between PC4 and 1,3-*trans*-PtTz-**III**. Significant decrease was also observed in the deuteration ratio of peptic peptides, Pep5 – Pep7 and Pep12 – Pep13, which arose from β3 – β5-sheets (I85 – L105) of the holo-PC4, compared to those of the apo-PC4 (Fig. 2 and S4 – S9). These revealed that β3 – β5-sheet region is also involved in the recognition and binding of PC4 to 1,3-PtTz-**III**. Peptic peptides Pep15 – Pep17, which cover residues W110 to D122, were derived from the only α-helix in PC4. Surprisingly, upon binding to 1,3-*trans*-PtTz-**III**, their maximum deuterium uptake number significantly increased compared to apo-PC4 (Fig. 2 and S10 – S12). These results indicated that the ligation of PC4 with 1,3-*trans*-PtTz-**III** did not occur on the dimerization interface of PC4 instead partially loosen the PC4 dimer by the ligation in the adjacent β-sheet region.[8,9]

Molecular dynamics simulations

Based on the results described above, the molecular mechanism of PC4 protein binding to 1,3-*trans*-PtTz-**III** was further investigated by means of molecular dynamics (MD) simulations. To this end, two molecular models of *trans*-PtTz binding with dsODN **III** were constructed. A common feature of both models lies in the fact that the Pt atom of *trans*-PtTz forms 1,3-GXG intrastrand crosslinking with G6 and G8 of the ODN, differing only in the thiazole group's orientation towards the ODN's exterior (DL_{out}) or interior (DL_{in}) (Supplementary Fig. S13a and b). Subsequently, we established a fully solvated structure with 0.15 M ion concentration, optimized it, and conducted 500 ns MD simulations on both systems, replicating each simulation three times. The simulations revealed that both DL_{out} and DL_{in} configurations of the 1,3-*trans*-PtTz-**III** complex remained stable (Supplementary Fig. S13c and d). Furthermore, the *trans*-PtTz binding significantly altered dsODN's conformation, causing the overall ODN chain thicker and shorter than the B-form dsODN. The G6-G8 region underwent significant deformation, disrupting the double helix structure and base pairing, whereas the double helix structure in the remaining region was preserved well (Supplementary Fig. S14 – S15).

The structure of the full-length PC4 protein has not yet been determined. The available structure contains only the residue sequence of M63-L127 (PDB code: 2C62), while the segment of M1-M63 was considered to be disordered. Our HDX-MS experiments suggested that segment R47-M63 is involved in the binding of 1,3-*trans*-PtTz-**III**, while segment M1-S46 does not seem to be associated with the binding

of DNA. Therefore, AlphaFold2[35] and tFold[36] were used to predict the structure of R47-L127. The predicted structure of M63-L127 resembles the X-ray crystallographic structure (PDB code: 2C62), while the R47-M63 segment adopts a coiled-coil configuration predicted by AlphaFold 2 (Supplementary Fig. S16).

Our global HDX-MS results indicate that PC4 binds to 1,3-*trans*-PtTz-**III** in a 1:1 stoichiometric ratio. As literature reported that the C-terminal structural domain of PC4 usually dimerizes to accommodate single-stranded DNA under physiological conditions,[8-10] we explored the scenario where the PC4 dimer binds to two 1,3-*trans*-PtTz-**III** monomers (2:2) using MD simulations. This resulted in four possible complexes, holo-PC4-1 to holo-PC4-4 shown in Supplementary Fig. S17. For each complex, we constructed a fully hydrated system with an concentration of 0.15 M using Hdock[37], performed energy minimization and equilibrium treatments, and conducted MD simulations for up to 100 nanoseconds (ns). The RMSD (root mean square deviation) data of the backbone indicates that all the four structures are relatively stable (Supplementary Fig. S18), so the last 50 ns trajectory of each system's simulation was used for further data analysis.

The solvent accessible surface area (SASA) of PC4 in each structure model of holo-PC4 (1,3-*trans*-PtTz-**III**-PC4) were monitored (Fig. 3a and Supplementary Fig. S19). After binding to 1,3-*trans*-PtTz-**III**, the SASA of both the serine-rich segment R47-M63 and the K80-Q109 regions on the β-sheet of holo-PC4 were reduced compared to apo-PC4, demonstrating that these two regions are involved in the interaction with 1,3-*trans*-PtTz-**III**. In contrast, the SASA of the C-terminal α-helical dimer (W110-D122) of holo-PC4 increased compared to that in apo-PC4, presumably due to the partial disruption of the stacking within the dimer due to hosting the 1,3-*trans*-PtTz-**III** complex. Unambiguously, the trends of residue exposure changes for all four models were consistent with the HDX-MS results described aforementioned, which partially confirmed the validity of the structural models.

The four holo-PC4 models were further examined with respect to their energy. Among these models, holo-PC4-2 has the highest interaction energy of −139.64 kcal/mol, showing the strongest binding tendency (Table 2 and Table S1). In addition, the potential energy of holo-PC4-2 was also the lowest among the four structures (Supplementary Fig. S20). Accordingly, we focused on the conformation of holo-PC4-2 to study the mechanism underlying the interaction of the Pt-crosslinked dsODN and PC4. In holo-PC4-2 model, each of the two 1,3-*trans*-PtTz-**III** molecules bound to the cavity formed by β-sheets (residue ID: 64-109) in one subunit of PC4 dimer and was further wrapped by the coiled-coil N-terminal segment of PC4 (Fig. 3b). This is consistent with the HDX-MS results. The positively charged residue-rich segment R47-M63 has favorable electrostatic attractions with the phosphate group of the dsODN. However, the binding of R47-M63 to 1,3-*trans*-PtTz-**III** is nonspecific, as shown by the trajectory of MD simulations. In contrast, the dsODN specifically interacts with the cavities of PC4. As shown in Table S2 and Fig. 4b, K78 and K80 on β2, R86 on β3, and R100 on β5 formed stable hydrogen bonds with 1,3-*trans*-PtTz-**III**, respectively. K101 stably binds to the 1,3-*trans*-PtTz-**III** accommodated by another subunit of PC4 dimer with a hydrogen bonding occupancy of more than 50%. In contrast, R100 can either bind to the 1,3-*trans*-PtTz-**III** within the hosting subunit or to the 1,3-*trans*-PtTz-**III** on the neighboring subunit.

Notably, R86 stably interacted with 1,3-*trans*-PtTz-**III** within each subunit, and the occupancy of the direct hydrogen bonding was up to 60%.

Through the analysis of the overall structure of the PC4-1,3-*trans*-PtTz-**III** complex, we found that there are two interlocking stacked V-shaped segments in PC4 dimer, each of which is composed of β-sheets and the α-helix in the same subunit to form the two edges of the V-shaped configuration (Fig. 3c). The former domain, the major component of the cavity, binds to dsODN with some positively charged residues, such as K78, K80, R86, and R100. The latter, the α-helix (residues 110-127) at the C-terminus of the PC4, has extensive hydrophobic interactions with the β-sheet of another subunit and thus changed accordingly with the conformational change of the β-sheet. Therefore, the conformational changes of PC4 due to DNA binding can be directly characterized by studying the changes in the angle of the clamp of this V-shaped structure. The angles in both V-shapes in holo-PC4-2 decreased compared to apo-PC4, which indicates that the binding of dsODN leads to an overall contraction of the protein (Fig. 3d and Supplementary Fig. S21). The distance between the α-helical fragments at the C-terminus of the PC4 increased due to dsODN binding by monitoring the closest distance between the residue atoms in the holo-PC4-2 and apo-PC4 dimeric portions (Fig. 3e and Supplementary Fig. S21). This agrees with the above results for SASA analysis (Fig. 3a). It appears that the synergistic interaction between the two units of PC4 leads to the loosening of the C-terminal stacking α-helices.

To further illustrate the contribution of R86 toward binding, we mutated it to Ala (A) residue and performed another 100 ns MD simulations. The PC4-R86A system exhibited detachment of 1,3-*trans*-PtTz-**III** from the cavity (Supplementary Fig. S22), and the decreased binding free energy after mutation further illustrated the key role of R86 (Table 2 and Table S1).

Table 2. The binding free energies calculated using MM/PBSA for four holo-PC4 and mutated holo-PC4R86A with 1,3-*trans*-PtTz-**III**. All energies are in kcal/mol, and all errors are square deviations. $\Delta\Delta G_{binding}$ is the difference between $\Delta G_{binding}$ for mutated holo-PC4-n and holo-PC4-n, where n is the model index.

	holo-PC4-1	holo-PC4-2	holo-PC4-3	holo-PC4-4
$\Delta G_{binding}$	−88.68±24.86	−139.64±24.49	−61.38±24.81	−78.57±22.94
$\Delta\Delta G_{binding}$	39.96	17.58	29.53	77.94

Electrophoretic mobility shift assays (EMSAs)

EMSAs were performed to provide an additional support to binding sites at single amino acid residue level for the interaction of PC4 with the platinated dsODN **III**. Fluorescein-labeled single-stranded **II** (**F-II**) was used to produce fluorescent 1,3-*trans*-PtTz-**III** complex. EMSAs were respectively run for platinated **III** complex, intact dsODN **III** and three types of PC4 proteins, i.e. wild-type PC4, site-directed mutants PC4R86A and PC4S104P. As shown in Fig. 4a and 4d, when the molar ratio of the wild type PC4 versus 1,3-*trans*-PtTz-**III** was raised to 8:1 or above, the lagging bands of the platinated ODN were observed. For

comparison, for the non-platinated **III** the lagging band did not occur until the molar ratio reached 12:1. This indicates that PC4 binds to 1,3-*trans*-PtTz-**III** stronger than to non-platinated **III**.

In the presence of PC4R86A mutant, lagging band was not observed for 1,3-*trans*-PtTz-**III** until the molar ratio of protein to dsODN reached 128:1 (Fig. 4b, e). Whereas pronounced lagging band of the intact dsODN **III** arose when the molar ratio of PC4R86A mutant versus **III** was higher than 48:1. This suggests that the mutation at Arg86 significantly impeded the interaction of PC4 with the platinated ODN, but less impacted on the interaction between PC4 and the native double-stranded ODN. In other words, the Arg86 residue play a crucial role in the recognition and interaction of PC4 with 1,3-*trans*-PtTz-**III**. When Ser104 of PC4 was mutated to proline, the lagging band for both the platinated and non-platinated **III** appeared when the molar ratio of PC4S104P versus 1,3-*trans*-PtTz-**III** or intact **III** was higher than 24:1 (Fig. 4c, f), indicating that the S104P mutation also reduced the binding affinity of PC4 with ODN, but did not discriminate 1,3-*trans*-PtTz crosslinked **III** and the intact **III**.

The mutation of Arg86 of PC4 to Gly in A549 cells

To verify further the critical role of residue Arg86 in mediating the interaction of PC4 with the platinated dsODN **III**, the arginine residue located at position 86 of PC4 was mutated from arginine to glycine in A549 human non-small cell lung cancer cells via CRISPR/Cas9 editing. The cells expressed mutated PC4R86G were designated as A549/PC4R86G cells, and a control cell line, named A549/NC, was also cultured without adding sgRNA during CRISPR-Cas9 editing. The whole cell proteins were then extracted from the two cell lines, and UHPLC-tandem mass spectrometry analysis was then applied to verify the expression of PC4R86G mutant. As shown in Supplementary Fig. S23, the MS/MS spectra demonstrated the success of mutation at amino acid residue 86 from arginine to glycine in A549/PC4R86G cells, while in A549/NC cells, PC4wt was expressed. More importantly, the cell proliferation assays showed that the cytotoxicity indicated by IC_{50} value of *trans*-PtTz against the A549/NC cells treated for 24 h was 64.6±1.6 μM, while the IC_{50} value of *trans*-PtTz against A549/PC4R86G cells was 55.6±1.5 μM (Fig. 4g). This suggests that when Arg86 is mutated to glycine, the A549 cells become more sensitive to *trans*-PtTz.

Next, capase-6 serving as an indicator of cellular DNA damage and apoptosis,[38] were imaged by immunofluorescence microscopy in both A549/NC cells and A549/PC4R86G cells after treatment with 30 μM *trans*-PtTz for 24 h,. The images and Pearson's correlation coefficient of caspase-6 with DAPI, a cell nucleus dye, suggested that in A549/NC cells, the majority of caspase-6 was located in the cytoplasm region, whereas in A549/PC4R86G cells, caspase-6 mainly enters the nucleus (Fig. 4h and 4i). This demonstrated that the mutation of arginine to glycine at position 86 of PC4 deprives the ability of PC4 mediated DNA damage repair, thereby enhances cell apoptosis induced by *trans*-PtTz. This is in consistent with our previous work where PC4 was silenced by siRNA.[24]

Discussion

The human positive cofactor 4 (PC4) contains two major domains: the DNA-binding C-terminal domain (M63 – L127) and the flexible serine- or lysine-rich regulatory domain at the N-terminal (M1 – N62).[13,14] The conserved C-terminal, consisting of a curved five pieces of anti-parallel β-sheets followed by a 45° kinked α-helix, is essential for its functions in binding to ssDNA, which in turn transduces the repair signal of DNA damage and maintains genome stability.[15,39-41]

In previous reports, the crystal structure of PC4 showed that the C-terminal domain tends to form homodimers, in which two ssDNA binding channels can be formed in opposite direction.[8,9,42] The kinked α-helix, packing against the β-sheets of their respective dimeric partner, forms the central hydrophobic core, favoring the binding of ssDNA as well as the unwound complementary strands or mismatch heteroduplex DNA. The present work is the first report, to our best knowledge, to describe the structure basis of the recognition and interaction between PC4 and a platinum complex damaged double-stranded ODN. HDX-MS and MD simulations were applied to elucidate the binding site and interface of each monomer of the PC4 dimer to one 1,3-*trans*-PtTz-**III** molecule, revealing conformational changes and specific amino acid interactions within PC4 with the platinated dsODN. Results from both HDX-MS and MD simulations both suggested that the R47 – M63 residues at the serine-rich loop and K80 – Q109 at the β-sheet region of PC4 were involved in the interactions of PC4 with the *trans*-platinum complex crosslinked dsODN. The 1,3-*trans*-PtTz-**III** binding leads to an overall contraction of PC4, suggesting that PC4 units' synergistic interaction causes the slight separation of the C-terminal α-helices stacking. Specifically, K78, K80, R86, and R100, of the b3 – b5-sheets in PC4, formed stable H-bonds with the dsODN backbone phosphate groups, and played a crucial role in the unique interaction between PC4 and 1,3-*trans*-PtTz-**III**.

Notably, Arg86 on β3 stably interacts with 1,3-*trans*-PtTz-**III** within each subunit, exhibiting a direct hydrogen bond with a highest occupancy, which underscores a robust and consistent interaction. Site-directed mutation from R86 to other amino acid such as Ala or Gly were performed. Both MD simulations and electrophoretic assay suggested that mutation at Arg86 significantly impeded the interaction of PC4 with the platinated dsODN. Moreover, the key role of R86 was further extended to A549 human non-small-cell lung cancer cells. Mutation of the arginine amino acid residue to glycine directly caused increased damage of DNA accumulating in nuclei and enhanced the sensitivity of A549 cells towards *trans*-PtTz.

On the other hand, given that PC4 is an early responding protein to DNA damage, the results in this work implies that the recognition of the transplatin-induced lesions on DNA may initiate DNA repair, which in turn recovers DNA replication and transcription, diminishing the cytotoxicity of this *trans*-platinum complex. Indeed, recently we discovered that the downregulation or silencing of PC4 could promote the cytotoxicity of *trans*-PtTz.[24] This provides novel insights into improving the cytotoxicity of the *trans*-platinum complex to overcome the resistance of cancer cells to cisplatin.

Importantly, the N-terminal of PC4, although being a highly flexible and unstructured serine- and lysine-rich domain, can still play regulatory role. The mechanism was previously believed to be modulation

and/or shielding of the interaction surface of the structured C-terminal core domain.[34] The non-specific but moderate electrostatic attraction of serine residues in R47 – M63 region with the phosphate group of DNA was also revealed by both HDX-MS analysis and molecular dynamics simulation in our work, showing that the previous overlooked flexible domain can also be involved in the unique interaction of PC4 with the 1,3-*trans*-PtTz crosslinked dsODN.

Significantly, our studies herein reveal a totally different mechanism of action for PC4 recognizing and binding to *trans*-PtTz-crosslinked DNA from that of the high mobility group box 1 (HMGB1) protein, which is a reader and binder of cisplatin crosslinked DNA. HMGB1 has been extensively explored and shown to shield cisplatin damaged DNA from repair, and as a consequence enhancing cisplatin cytotoxicity.[12,19] Moreover, HMGB1 has also been reported as a mediator for tumor antigen-specific response in immunogenic cell death.[43] These unique functions of DNA binding proteins imply crucial roles of downstream responses of intracellular proteins in regulating anticancer activity of DNA targeting drugs.

In summary, hydrogen/deuterium exchange mass spectrometry (HDX-MS) combined with online pepsin digestion and molecular dynamics simulations has been applied herein to study the molecular mechanism for the unique recognition and interaction of PC4 protein with 1,3-GTG intrastrand crosslinked dsODN by *trans*-PtTz. HDX-MS data and MD simulation revealed network of electrostatic and hydrophobic interactions between PC4 and 1,3-*trans*-PtTz crosslinked dsODN in a 2:2 manner. The three b3 – b5-sheets (especially I85 – L105 residues) in PC4 were shown to be interaction interface. The amino acid residues K78, K80, R86 and R100 form stable hydrogen bonds with 1,3-*trans*-PtTz-**III** in each PC4 monomer, while the amino acid K101 formed a stable hydrogen bond with the Pt-crosslinked dsODN complex bound to another monomer of PC4. Importantly, the Arg86 residues in the interaction interface was demonstrated to be the dominant binding site of PC4 to 1,3-*trans*-PtTz-**III.** The site-directed mutation at Arg86 to Gly reduced the affinity of PC4 to the platinated dsODN in vitro and promoted the cytotoxicity of *trans*-PtTz against human A549 lang cancer cells, implying that PC4 binding mediates the repair of *trans*-PtTz crosslinked DNA, unfavorable to the anticancer activity of the *trans*-platinum complex. The structural basis for the interaction of PC4 with *trans*-platinum damaged DNA provided novel insights into elucidating the regulatory effect of PC4 on the repair of *trans*-PtTz damaged DNA. On the other hand, the successful application of the method by combining HDX-MS with online pepsin digestions and molecular dynamics simulations can be further widely applied to study the interactions between other intact or/and damaged DNA and proteins.

Declarations

Online content

Any methods, additional references, Nature Portfolio reporting summaries, source data, extended data, supplementary information, acknowledgements, peer review information; details of author contributions and competing interests; and statements of data and code availability are available at https://doi.org/

Conflicts of interest

There are no conflicts to declare.

Additional information

Supplementary information The online version contains supplementary material available at https://doi.org/

Correspondence and requests for materials should be addressed to Fuyi Wang, Hao Dong and Yao Zhao.

Author Contributions

F.W. H.D. and Y.Z. conceived, designed and supervised the project. Y.W., Z.D., K.W., W.Z. and Q.L. performed the HDX-MS and EMSA experiments. M.Z. and H.D. performed the molecular simulations. J.Q. and L.Q. fabricated the online pepsin digestion column. Y.H. and Q.L. performed analysis with A549/PC4R86G cell line. Y.W., Z.D., F.W., H.D. and Y.Z. analysed data, wrote and revised the manuscript.

Acknowledgements

We thank the National Natural Science Foundation of China (grant No. 22377130, 22273034, 22361142831), Beijing Natural Science Foundation (grant No. 2232034) and the Scientific Instrument Developing Project of the Chinese Academy of Sciences (grant No. PTYQ2024TD0012) for support. Parts of the calculations were performed using computational resources on an IBM Blade cluster system from the High-Performance Computing Center (HPCC) of Nanjing University. We thank Professor Yangzhong Liu of University of Science and Technology of China for providing the *trans*-PtTz complex as a gift.

Data availability

The data supporting the findings of this study are available within the paper and its Supplementary Information. Should any raw data files be needed in another format, they are available from the corresponding author upon reasonable request. Source data are provided with this paper.

References

1. Kaypee, S. et al. Positive coactivator PC4 shows dynamic nucleolar distribution required for rDNA transcription and protein synthesis. *Cell Commun Signal* **23**, 283 (2025).

2. Dubois, J.C. et al. The single-stranded DNA-binding factor SUB1/PC4 alleviates replication stress at telomeres and is a vulnerability of ALT cancer cells. *Proc Natl Acad Sci U S A* **122**, e2419712122 (2025).
3. Pan, Q. et al. The SETDB1-PC4-UPF1 post-transcriptional machinery controls periodic degradation of CENPF mRNA and maintains mitotic progression. *Cell Death Differ* **32**, 1413-1427 (2025).
4. Salgado, S. et al. Human PC4 supports telomere stability and viability in cells utilizing the alternative lengthening of telomeres mechanism. *EMBO Rep* **25**, 5294-5315 (2024).
5. Pan, Q., Luo, P. & Shi, C. PC4-mediated Ku complex PARylation facilitates NHEJ-dependent DNA damage repair. *J Biol Chem* **299**, 105032 (2023).
6. Garavís, M. & Calvo, O. Sub1/PC4, a multifaceted factor: from transcription to genome stability. *Current Genetics* **63**, 1023-1035 (2017).
7. Tavenet, A. et al. Genome-wide location analysis reveals a role for Sub1 in RNA polymerase III transcription. *Proceedings of the National Academy of Sciences* **106**, 14265-14270 (2009).
8. Brandsen, J. et al. C-terminal domain of transcription cofactor PC4 reveals dimeric ssDNA binding site. *Nature Structural Biology* **4**, 900-903 (1997).
9. Werten, S. & Moras, D. A global transcription cofactor bound to juxtaposed strands of unwound DNA. *Nature Structural & Molecular Biology* **13**, 181-182 (2006).
10. Hyjek-Składanowska, M. et al. Origins of the Increased Affinity of Phosphorothioate-Modified Therapeutic Nucleic Acids for Proteins. *Journal of the American Chemical Society* **142**, 7456-7468 (2020).
11. Werten, S. et al. Interaction of PC4 with melted DNA inhibits transcription. *Embo Journal* **17**, 5103-5111 (1998).
12. Wang, D. & Lippard, S.J. Cellular processing of platinum anticancer drugs. *Nature Reviews Drug Discovery* **4**, 307-320 (2005).
13. Werten, S. et al. High-affinity DNA binding by the C-terminal domain of the transcriptional coactivator PC4 requires simultaneous interaction with two opposing unpaired strands and results in helix destabilization. *Journal of Molecular Biology* **276**, 367-377 (1998).
14. Kaiser, K., Stelzer, G. & Meisterernst, M. The coactivator P15 (PC4) initiates transcriptional activation during TFIIA-TFIID-promoter complex-formation. *Embo Journal* **14**, 3520-3527 (1995).
15. Batta, K., Yokokawa, M., Takeyasu, K. & Kundu, T.K. Human Transcriptional Coactivator PC4 Stimulates DNA End Joining and Activates DSB Repair Activity. *Journal of Molecular Biology* **385**, 788-799 (2009).
16. Mortusewicz, O. et al. Recruitment of RNA polymerase II cofactor PC4 to DNA damage sites. *Journal of Cell Biology* **183**, 769-776 (2008).
17. Jamieson, E.R. & Lippard, S.J. Structure, recognition, and processing of cisplatin-DNA adducts. *Chemical Reviews* **99**, 2467-2498 (1999).

18. Lin, Y. et al. Single cell imaging reveals cisplatin regulating interactions between transcription (co)factors and DNA. *Chemical Science* **12**, 5419-5429 (2021).
19. Jung, Y.W. & Lippard, S.J. Direct cellular responses to platinum-induced DNA damage. *Chemical Reviews* **107**, 1387-1407 (2007).
20. Perez, J.M., Fuertes, M.A., Alonso, C. & Navarro-Ranninger, C. Current status of the development of *trans*-platinum antitumor drugs. *Critical Reviews in Oncology Hematology* **35**, 109-120 (2000).
21. Suchankova, T., Vojtiskova, M., Reedijk, J., Brabec, V. & Kasparkova, J. DNA and glutathione interactions in cell-free media of asymmetric platinum(II) complexes *cis*- and *trans*-[$PtCl_2$(isopropylamine)(1-methylimidazole)]: relations to their different antitumor effects. *Journal of Biological Inorganic Chemistry* **14**, 75-87 (2009).
22. Marini, V. et al. Conformation, protein recognition and repair of DNA interstrand and intrastrand cross-links of antitumor *trans*-[$PtCl_2(NH_3)$(thiazole)]. *Nucleic Acids Research* **33**, 5819-5828 (2005).
23. Du, Z. et al. Mass Spectrometric Proteomics Reveals that Nuclear Protein Positive Cofactor PC4 Selectively Binds to Cross-Linked DNA by a *trans*-Platinum Anticancer Complex. *Journal of the American Chemical Society* **136**, 2948-2951 (2014).
24. Hou, Y. et al. G-quadruplex inducer/stabilizer pyridostatin targets SUB1 to promote cytotoxicity of a transplatinum complex. *Nucleic Acids Research* **50**, 3070–3082 (2022).
25. Chalmers, M.J., Busby, S.A., Pascal, B.D., West, G.M. & Griffin, P.R. Differential hydrogen/deuterium exchange mass spectrometry analysis of protein-ligand interactions. *Expert Review of Proteomics* **8**, 43-59 (2011).
26. Marciano, D.P., Dharmarajan, V. & Griffin, P.R. HDX-MS guided drug discovery: small molecules and biopharmaceuticals. *Current Opinion in Structural Biology* **28**, 105-111 (2014).
27. Rand, K.D., Zehl, M. & Jorgensen, T.J.D. Measuring the Hydrogen/Deuterium Exchange of Proteins at High Spatial Resolution by Mass Spectrometry: Overcoming Gas-Phase Hydrogen/Deuterium Scrambling. *Accounts of Chemical Research* **47**, 3018-3027 (2014).
28. Huang, L., So, P.-K., Chen, Y.W., Leung, Y.-C. & Yao, Z.-P. Conformational Dynamics of the Helix 10 Region as an Allosteric Site in Class A β-Lactamase Inhibitory Binding. *Journal of the American Chemical Society* **142**, 13756-13767 (2020).
29. Longbotham, J.E. et al. Histone H3 binding to the PHD1 domain of histone demethylase KDM5A enables active site remodeling. *Nature Communications* **10**(2019).
30. Trabjerg, E. et al. Investigating the Conformational Response of the Sortilin Receptor upon Binding Endogenous Peptide- and Protein Ligands by HDX-MS. *Structure* **27**, 1103-1113.e3 (2019).
31. Ye, X., Lin, J.B., Mayne, L., Shorter, J. & Englander, S.W. Hydrogen exchange reveals Hsp104 architecture, structural dynamics, and energetics in physiological solution. *Proceedings of the National Academy of Sciences of the United States of America* **116**, 7333-7342 (2019).
32. Poliakov, A., Jardine, P. & Prevelige, P.E. Hydrogen/deuterium exchange on protein solutions containing nucleic acids: utility of protamine sulfate. *Rapid Communications in Mass Spectrometry*

22, 2423-2428 (2008).

33. Yao, C., Qi, L., Hu, W., Wang, F. & Yang, G. Immobilization of trypsin on sub-micron skeletal polymer monolith. *Analytica Chimica Acta* **692**, 131-137 (2011).
34. Jonker, H.R.A., Wechselberger, R.W., Boelens, R., Kaptein, R. & Folkers, G.E. The Intrinsically Unstructured Domain of PC4 Modulates the Activity of the Structured Core through Inter- and Intramolecular Interactions. *Biochemistry* **45**, 5067-5081 (2006).
35. Jumper, J. et al. Highly accurate protein structure prediction with AlphaFold. *nature* **596**, 583-589 (2021).
36. Xiao, Q. et al. Structure of human steroid 5α-reductase 2 with the anti-androgen drug finasteride. *Nature communications* **11**, 5430 (2020).
37. Yan, Y., Zhang, D., Zhou, P., Li, B. & Huang, S.-Y. HDOCK: a web server for protein–protein and protein–DNA/RNA docking based on a hybrid strategy. *Nucleic acids research* **45**, W365-W373 (2017).
38. Zheng, M., Karki, R., Vogel, P. & Kanneganti, T.-D. Caspase-6 Is a Key Regulator of Innate Immunity, Inflammasome Activation, and Host Defense. *Cell* **181**, 674-687.e13 (2020).
39. Mortusewicz, O., Evers, B. & Helleday, T. PC4 promotes genome stability and DNA repair through binding of ssDNA at DNA damage sites. *Oncogene* **35**, 761-70 (2016).
40. Caldwell, R.B. et al. Positive Cofactor 4 (PC4) is critical for DNA repair pathway re-routing in DT40 cells. *Scientific Reports* **6**(2016).
41. Wang, J.Y., Sarker, A.H., Cooper, P.K. & Volker, M.R. The single-strand DNA binding activity of human PC4 prevents mutagenesis and killing by oxidative DNA damage. *Molecular and Cellular Biology* **24**, 6084-6093 (2004).
42. Werten, S., Wechselberger, R., Boelens, R., van der Vliet, P.C. & Kaptein, R. Identification of the Single-stranded DNA Binding Surface of the Transcriptional Coactivator PC4 by NMR. *Journal of Biological Chemistry* **274**, 3693-3699 (1999).
43. Englinger, B. et al. Metal Drugs and the Anticancer Immune Response. *Chemical Reviews* **119**, 1519-1624 (2019).
44. Vanbeusichem, M. & Farrell, N. Activation of the trans geometry in platinum antitumor complexes - synthesis, characterization, and biological - activity of complexes with the planar ligands pyridine, N-methylimidazole, thiazole, and quinoline - crystal and molecular - structure of *trans*-dichlorobis(thiazole) platinum(II). *Inorganic Chemistry* **31**, 634-639 (1992).
45. Jiang, T., Jiskra, J., Claessens, H.A. & Cramers, C.A. Preparation and characterization of monolithic polymer columns for capillary electrochromatography. *Journal of Chromatography A* **923**, 215-227 (2001).
46. Guttman, M., Weis, D.D., Engen, J.R. & Lee, K.K. Analysis of Overlapped and Noisy Hydrogen/Deuterium Exchange Mass Spectra. *Journal of the American Society for Mass Spectrometry* **24**, 1906-1912 (2013).

47. Case, D. et al. AMBER16 package. *University of California* (2016).
48. Frisch, M. et al. Gaussian 16, Gaussian. *Inc., Wallingford CT* **2016**(2016).
49. Franchini, M., Philipsen, P.H.T., van Lenthe, E. & Visscher, L. Accurate Coulomb potentials for periodic and molecular systems through density fitting. *Journal of chemical theory and computation* **10**, 1994-2004 (2014).
50. Chiodo, S., Russo, N. & Sicilia, E. LANL2DZ basis sets recontracted in the framework of density functional theory. *The Journal of chemical physics* **125**(2006).
51. Mitin, A.V., Baker, J. & Pulay, P. An improved 6-31 G* basis set for first-row transition metals. *The journal of chemical physics* **118**, 7775-7782 (2003).
52. Phillips, J.C. et al. Scalable molecular dynamics with NAMD. *Journal of computational chemistry* **26**, 1781-1802 (2005).
53. Wang, J., Wolf, R.M., Caldwell, J.W., Kollman, P.A. & Case, D.A. Development and testing of a general amber force field. *Journal of Computational Chemistry* **25**, 1157-1174 (2004).
54. Darden, T., York, D. & Pedersen, L. Particle mesh Ewald: An N log (N) method for Ewald sums in large systems. *Journal of chemical physics* **98**, 10089-10089 (1993).
55. Miyamoto, S. & Kollman, P.A. Settle: An analytical version of the SHAKE and RATTLE algorithm for rigid water models. *Journal of computational chemistry* **13**, 952-962 (1992).
56. Lavery, R., Moakher, M., Maddocks, J.H., Petkeviciute, D. & Zakrzewska, K. Conformational analysis of nucleic acids revisited: Curves+. *Nucleic acids research* **37**, 5917-5929 (2009).
57. Liu, H. & Hou, T. CaFE: a tool for binding affinity prediction using end-point free energy methods. *Bioinformatics* **32**, 2216-2218 (2016).
58. Humphrey, W., Dalke, A. & Schulten, K. VMD: visual molecular dynamics. *Journal of molecular graphics* **14**, 33-38 (1996).
59. Nash, J.C. *Compact numerical methods for computers: linear algebra and function minimisation*, (Routledge, 2018).
60. DeLano, W.L. Pymol: An open-source molecular graphics tool. *CCP4 Newsl. protein crystallogr* **40**, 82-92 (2002).
61. Du, Z.F. et al. Mass Spectrometric Proteomics Reveals that Nuclear Protein Positive Cofactor PC4 Selectively Binds to Cross-Linked DNA by a trans-Platinum Anticancer Complex. *Journal of the American Chemical Society* **136**, 2948-2951 (2014).

Methods

Starting materials

trans-[$PtCl_2(NH_3)$(thiazole)] (*trans*-PtTz; Fig. 1a) was prepared following the procedure reported previously.[44] The recombinant PC4 protein was obtained from Proteintech (Wuhan, China). The sequence of human PC4 protein was adopted from Uniprot database align No.: P53999. Pepsinogen

was purchased from Sigma-Aldrich and used without further purification. Deuterium oxide (99.9%), formic acid (FA) and protamine sulfate were all purchased from Sigma. The complementary single-stranded oligodeoxynucleotides (ODNs) 5¢-CTCTTGTGTTCTTCT-3¢, (**I**) and 5¢-AGAAGAACACAAGAG-3¢ (**II**) were obtained from TaKaRa (Dalian, China; Fig. 1b). The HPLC-grade solvents (water and acetonitrile) for mobile phases used in MS and HPLC were all purchased from ThermoFisher (USA). All aqueous solutions used in this work were prepared using di-ionized water from Milli-Q Reagent Water System.

Preparation of platinated dsODN

The 1,3-GTG intrastrand crosslinked single-stranded ODN **I** by *trans*-PtTz and the dsODN containing the *trans*-PtTz damage site was prepared following the procedure described in the our previous report.[23] Briefly, *trans*-PtTz was incubated with the -GTG-containing single-stranded **I** at a molar ratio of 0.8:1 at 37 °C for 3 days. Then the 1,3-GTG intrastrand crosslinked strand **I** was purified by HPLC with a C8 column (4.6 × 250 mm, 5 µm, Agilent) on an Agilent 1200 HPLC system where the mobile phases were water containing 20 mM TEAA and acetonitrile containing 20 mM TEAA. The purified *trans*-PtTz 1,3-GTG intrastrand crosslinked ODN **I** was characterized by ESI-MS and quantified by UV-visible spectrometer and then lyophilized. Thereafter, the platinated ODN I mixed with equal mole of the complementary strand **II** in 100 mM $NaClO_4$ was heated to 85 °C, sustained for 5 min and cooled slowly to room temperature. The formed *trans*-PtTz 1,3-GTG intrastrand crosslinked double-stranded ODN **III** (1,3-*trans*-PtTz-**III**) was stored at –20 °C before use.

H/D exchange protocol

The aqueous solution of recombinant PC4 (100 mM) were prepared in 20 mM HEPES (pH 7.4) containing 100 mM NaCl. Titration experiments started with the equilibration of PC4 (100 mM) with varying concentrations of 1,3-*trans*-PtTz-**III** in more than 2 h.

For global deuterium uptake, the apo-PC4 (free intact protein) was incubated with 2 equiv. mol of 1,3-*trans*-PtTz-**III** in buffer containing 20 mM HEPES and 200 mM NaCl (pH 7.4) at 295 K for 120 min to give holo-PC4 (1,3-*trans*-PtTz-**III**-PC4). Aliquot (9 µL) of D_2O was added to 1 µL of apo-PC4 and holo-PC4, respectively, to initiate H/D exchange, where the final concentration ofD_2O was 90% (v/v). After various incubation time, the HDX was quenched with 1 µL ice-cold FA (20%) (holo-PC4 sample also containing 10:1 mol equiv. of protamine sulfate and 1,3-*trans*-PtTz-**III**) to give a final pH of 2.5. Protamine sulfate was used to remove excess of platinated ODN from the ODN **III**-PC4 complexes prior to MS analysis. Deuterated protein was loaded immediately on an Inertsil WP300 C8 column (2.1 ´ 50 mm, 5 µm, GL Sciences) and separated with use of mobile phase A (0.1% FA in water) and B (0.1% FA in acetonitrile). A gradient from 10% – 60% B within 6 min at 2 ± 0.2 °C was used to elute the proteins directly into the mass spectrometer for analysis.

To determine the local deuterium uptake, a house-made online pepsin digestion column applied in the HPLC system coupled with ESI-MS was developed. The online pepsin digestion column was fabricated

by immobilizing the pepsinogen on sub-micron skeletal polymer monolith as previously reported.[33] The residual epoxide groups were blocked by 1 mg mL^{-1} aspartic acid in 50 mM Tris-HCl buffer (pH 7.5) for 1 h. The immobilized pepsinogen column was activated by 10 column volumes of 0.1% FA (pH 2.5) passing through the column prior to incubating with 2 mg mL^{-1} soluble porcine pepsin for 16 h at 37 °C.[45] Then the activated pepsinogen column was rinsed with 50 column volumes of 0.1% FA (pH 2.5) to remove non-immobilized pepsin prior to use. The mixture of PC4 and platinated dsODN **III** in 90% D_2O was quenched with 20% FA after deuterium exchange for requested times and then injected into the system using valve A (Rheodyne valve Model 7725i) equipped with a 10-μL loop maintained at 2 ± 0.2 °C. This injector was connected to a column (4.6 ´ 50 mm) packed with immobilized pepsin. Mobile phase (0.1% FA, pH 2.5, flow rate 210 μL min^{-1}) from pump C (LC-20AD, Shimadzu) carried the protein from the injection loop to the pepsin column where the protein was digested into peptides at 2 ± 0.2 °C. The same mobile phase carried the peptides to a trap column (C18, 4.6 ´ 20 mm; Waters) where the D-labeled peptides were desalted and concentrated. Mobile phases A (0.1% FA/H_2O) and B (0.1% FA/acetonitrile) were applied to separate the peptides from the trap column through valve B (Rheodyne 7000 switching valve, Scheme 1) and the HPLC column (Ultimate AQ-C18, 2.1 ´ 50 mm, 5 μm, Welch) to the ESI-MS probe. A gradient from 15% to 50% of mobile phase B in 6 min was used for peptide separation. When deuterated samples were analyzed, part of the system, including the valves A and B, the sample loop, the pepsin column, the C18 trap column and the analytical column were all maintained at 2 ± 0.2 °C in the house-made precise temperature control refrigerator (50 ´ 50 ´ 50 cm^3) (refer to Scheme 1). The global or local deuterium uptake ratio was calculated by using equation 1 as follow.

$$\mathbf{Deuterium\%} = \frac{\boldsymbol{M_{HDX} - M_{control}}}{\boldsymbol{(N-2)\times 0.9}} \times \mathbf{100\%} \qquad (1)$$

where M_{HDX} is the centroid mass of a deuterated protein/peptide, $M_{control}$ is the centroid mass of the corresponding non-deuterated protein/peptide, N is the number of amino acids in the protein/peptide, (N − 2) is the number of exchangeable amide hydrogens, and 0.9 presents the final D_2O content of the buffer system.

Electrospray ionization mass spectrometry (ESI-MS)

Positive-ion ESI-MS were obtained on a Xevo G2 Q-TOF coupled to a Waters ACQUITY H-class HPLC system (Waters). The solvent tubes and columns were all maintained at 2 ± 0.2 °C to minimize back-exchange of amide hydrogen. The capillary voltage was 3 kV, sample cone 40 V and extraction cone 4 V. The desolvation temperature was 623 K and source temperature 373 K. Nitrogen was used as desolvation gas with a flow rate of 600 L h^{-1}. Global deuterium uptake spectra and local deuterium uptake spectra were acquired in the range of *m/z* 100 – 2000. All analysis were performed with “lockspray” to ensure accuracy and reproducibility. Leucine–enkephalin was used for the “lockmass” calibration at a concentration of 2 ng $μL^{-1}$ and flow rate of 10 μL min^{-1}. MS Data were collected in

continuum mode, the lockspray frequency was once every 10 s, and the data were averaged over 10 scans. MassLynx (ver. 4.1), Biopharmalynx (ver. 1.3) and HX-Express (ver. 2)[46] were used for data collection, analysis and processing.

System preparation for molecular simulations

Since the full-length crystal structure of PC4 is unavailable, we predicted the complete PC4 structure using AlphaFold2[35]. HDX-MS data showed that the disordered M1-S46 segment does not participate in binding with *trans*-PtTz-DNA (*vide infra*). Consequently, to reduce interference from the M1-S46 segment and the computational cost, we used the PDB structure of PC4 (M63-L127, PDB: 2C62)[9] and supplemented it with the AlphaFold2-predicted R47-P62 region, yielding a PC4 model spanning residues R47-L127.

The double-stranded DNA **III** (5′-d(CTCTTGTGTTCTTCT)-3′) was generated in the B-DNA conformation using the Nucleic Acid Builder in Amber16[47]. The T5-T9 segment was crosslinked with [*trans*-Pt(NH_3)(thiozole)]$^{2+}$ ([*trans*-PtTz]$^{2+}$), where Pt binds to the N7 atoms of G6 and G8 on the same strand. *Trans*-PtTz and the T5-T9 fragment were optimized with Gaussian 16[48] using the M06-2X[49] function, LANL2DZ[50] for Pt, and 6-31+G*[51] for C, N, S, and H atoms. The optimized fragment was embedded into the full dsODN **III** model to generate two initial 1,3-*trans*-PtTz-**III** complexes: DL_{in} (thiazole group of *trans*-PtTz oriented inward) and DL_{out} (thiazole group of *trans*-PtTz oriented outward). Each system was solvated with a 12 Å sphere 0.15 M NaCl solution in all directions. The DL_{in} and DL_{out} systems contained 31,954 and 30,562 atoms, respectively.

PC4 binding to the 1,3-*trans*-PtTz-**III** complex was modeled using HDOCK[37]. The second PC4 monomer was positioned via symmetry to assemble the holo-PC4 dimer binding to two 1,3-*trans*-PtTz-**III**. The entire complex was solvated in a 90 Å water box and neutralized with 62 Na^+ and 36 Cl^- ions. The final systems contained ~66,000 atoms, including the PC4 dimer (164 residues) and the 1,3-*trans*-PtTz-**III** complex (30 nucleotides, 4,592 atoms including the *trans*-PtTz).

Molecular dynamics simulations

For the 1,3-*trans*-PtTz-**III** systems, five rounds of 10,000-step energy minimization were performed to remove unfavorable contacts for relaxing water/ions, the G6-G8 and T5-T9 segments, the complementary A22-A26 region, and finally all dsODN **III** side chains. Equilibration then proceeded by gradually releasing harmonic restraints on T5-T9, A22-A26, the remaining dsODN **III** backbone/side chains, and the four terminal phosphates. To maintain the structure of the *trans*-PtTz moiety within dsODN **III**, collective-variable restraints of 90 kcal·mol^{-1}·Å^{-2} and 30 kcal·mol^{-1}·degree^{-2} were applied to the *trans*-PtTz unit and the corresponding guanine side chains in dsODN **III**, respectively. Post-equilibration, the system was subjected to a 500 ns MD sampling under NPT conditions at 1 bar and 300 K, and the last 100 ns of each of three independent replicas were used for analysis.

For the holo-PC4 complexes, initial minimization of energy was followed by equilibration with gradually reduced restraints on the side chains/backbones of both the 1,3-*trans*-PtTz-**III** adduct and PC4. The coordination between the platinum atom and the N7 atoms of G6 and G8 was restrained using the same force constants. All models were subsequently equilibrated for 100 ns under constant temperature (300 K) and pressure (1 bar) without restraints, with a time step of 0.5 fs, and the last 50 ns of the equilibrated trajectories were used for analysis.

All simulations were performed using the NAMD[52] software package with the AMBER force field[53]. Periodic boundary conditions were applied in all simulations. Long-range electrostatic interactions were treated with the particle mesh Ewald (PME) method[54], while a cutoff of 12 Å was used for short-range electrostatics and van der Waals interactions. All covalent bonds involving hydrogen atoms were constrained using the SHAKE algorithm[55].

The structural parameters of dsODN **III** and the 1,3-*trans*-PtTz-**III** adduct were analyzed using the CURVES program[56]. Binding free energies between PC4 and 1,3-*trans*-PtTz-**III** were calculated with the MM/PBSA method implemented in CaFE[57], based on 500 evenly spaced frames extracted from the equilibrated trajectories. Hydrogen bonds were identified using the Hbonds plugin in VMD[58]. Direct hydrogen bonds were defined as those with donor-acceptor distance < 3.5 Å and donor-hydrogen-acceptor angle > 150°, whereas indirect hydrogen bonds required the donor- acceptor distances to be < 3.8 Å. V-shaped structural angles were computed using the Orient module in VMD[58] in combination with the La linear algebra package in Hume[59]. Given the unique conformational rigidity of Pro107 relative to other amino acids, Pro107 was selected as the vertex of the V-shape. The angle between the principal Z inertia axes of the β-sheet (excluding the loop region) and the α-helix was then calculated to define the V-shaped geometry. VMD[58] and PyMOL[60] were used for MD trajectory analysis and molecular visualization.

Electrophoretic mobility shift assay

Fluorescein-labeled single-stranded ODN **II**, designated as **F-II**, was obtained from Sangon Biotech (Shanghai, China). Fluorescein-labeled 1,3-*trans*-PtTz-**III** was produced by annealing the 1,3-*trans*-PtTz platinated **I** with 1 mol equiv. of **F-II**. For EMSA experiments, aliquot (1 mL) of the fluorescent labeled 1,3-*trans*-PtTz-**III** (1 mM) was mixed with various volumes of recombinant PC4 protein (45 mM) or the same concentration of site-mutated PC4 (PC4A86A and PC4S104P, respectively), and the binding buffer (20 mM HEPES, 100 mM NaCl (pH 7.4) and 10 % (w/v) glycerol) was then added to make a final volume of 10 mL. The mixtures were incubated at room temperature for 2 h prior to sampling. The protein-ODN complexes were separated in 6% non-denaturing polyacrylamide gels in 1× Tris-borate-EDTA buffer (pH 8.1) run at 50 V at 4 °C for 60 min. After electrophoresis, the gels were imaged at excitation wavelength 488 nm and recorded at 600 nm with a Typhoon TRIO Variable Mode Imager (GE Health).

Site-directed mutation of PC4 expressed in A549 cells

The site-directed mutation of Arg86 to Gly86 in PC4 *via* CRISPR-Cas9 editing of *SUB1* gene, which encodes PC4, in human A549 lung cancer cells was performed by GenScript Inc. (Nanjing). The modified gene was successfully sequenced. The A549 cells expressing mutated PC4R86G protein, designated as A549/PC4R86G, and the A549 cells expressing wide-type PC4 protein (PC4wt), designated as A549/NC, were individually cultured in RPMI 1640 complete medium with 10% FBS. A549/NC was a negative control cell line without adding sgRNA during CRISPR-Cas9 editing. The two cell lines were respectively harvested, lysed on ice, and whole cell proteins were then extracted by total protein extraction kit (BestBio), and the total concentration of raw protein extracts was measured by BCA Kit (Beyotime).

Identification of PC4wt and PC4R86G by mass spectrometry

Proteins extracted from A549/PC4R86G cells and A549/NC cells were individually analyzed by mass spectrometry to verify the mutation of Arg86 in PC4. The denaturation, tryptic digestion of the proteins and the desalting of tryptic peptides were carried out by following the procedures reported in our previous work.[24,61]

Mass spectrometric analysis for the tryptic peptides was performed on an Orbitrap Fusion Lumos mass spectrometer coupled with an EASY-nLC 1200 nanoUPLC system equipped with an Acclaim™ PepMap™ 100 pre-column (20 mm × 75 μm, 3 μm) and an Acclaim™ PepMap™ RSLC C18 analytical column (150 mm × 75 μm, 2 μm). The UPLC mobile phase A was water containing 0.1% FA, and phase B 80% (vol/vol) methanol/water containing 0.1% FA. The desalted peptides were dissolved with phase A before injected to the UPLC. The gradient for UPLC separation started with 2% B and increased to 7% at 7 min, then to 20% at 69 min, 35% at 90 min and sharply to 95% within 5 min, maintained for 4 min, and finally decreased to 2% within 8 min and maintained for 3 min. The elution from the analytical column was directly infused to the mass spectrometer for MS/MS analysis.

Raw MS and MS/MS data were searched in Proteome Discoverer (Thermo Scientific, version 2.3) database for peptide and protein identification. Sequest HT search engine was used for peptides spectrum matching (PSM). The dynamic modifications were oxidation at methionine, methylation at lysine, glutarnine and arginine, acetylation at lysine and serine, phosphorylation at serine, threonine and tyrosine. The static modifications were carbamidomethylation at cysteine.

Inhibition of Cell Proliferation

A549/PC4R86G and A549/NC cells were respectively inoculated into a 96-well plate to achieve a cell density of 80-90%. The cells were then washed twice with PBS, followed by the cell proliferation inhibition experiments using *trans*-PtTz. The concentration gradients of *trans*-PtTz were 10, 30, 50, 60, 70, 75, 80, 85, 90, 95, 100, and 150 μM. After incubation cells with various concentrations of *trans*-PtTz at 37°C for 24 hours, 10 μL of CCK-8 reagent was added to each well, followed by an additional incubation at 37°C for 3 hours. Subsequently, the absorbance at 450 nm was measured, and based on this measurement, the IC50 value was calculated. The IC_{50} value represents the concentration of *trans*-PtTz required to inhibit cell growth by 50%.

Immunofluorescence Imaging Experiment

A549/PC4R86G and A549/NC cells were individually cultured in DMEM medium at a temperature of 37°C with a CO_2 concentration of 5%. The cells were treated with 30 μM *trans*-PtTz for 24 hours, then fixed with carnoy's reagent (methanol: acetic acid = 3:1) at -20°C for 10 minutes, followed by washing with PBS three times, each for 5 minutes. Subsequently, the cells were permeabilized with 0.1% Triton-X100/PBS at 37°C for 30 minutes, followed by blocking with 5% BSA/0.2% Triton X-100 PBS at the same temperature for 1 hour. Afterward, Cleaved Caspase-6 (Asp162) Antibody (CST, #9761) diluted in the blocking solution was incubated with the cells at 37°C for 1 hour. The cells were then washed three times with 0.2% BSA/0.02% Triton X-100 PBS on a decolorizing shaker, each time for 5 minutes. This was followed by incubation with Donkey Anti-Rabbit IgG H&L (Alexa Fluor 488) antibody (abcam, ab150073) at 37°C for 1 hour, and again washing the cells three times with 0.2% BSA/0.02% Triton X-100 PBS on a decolorizing shaker, each time for 5 minutes, and finally washing with PBS for 5 minutes before laser confocal imaging (Leica-Microsystems TCS SP8). The excitation and emission wavelengths were 495 nm and 519 nm, respectively.

Reporting summary

Further information on research design is available in the Nature Portfolio Reporting Summary linked to this article.

Figures

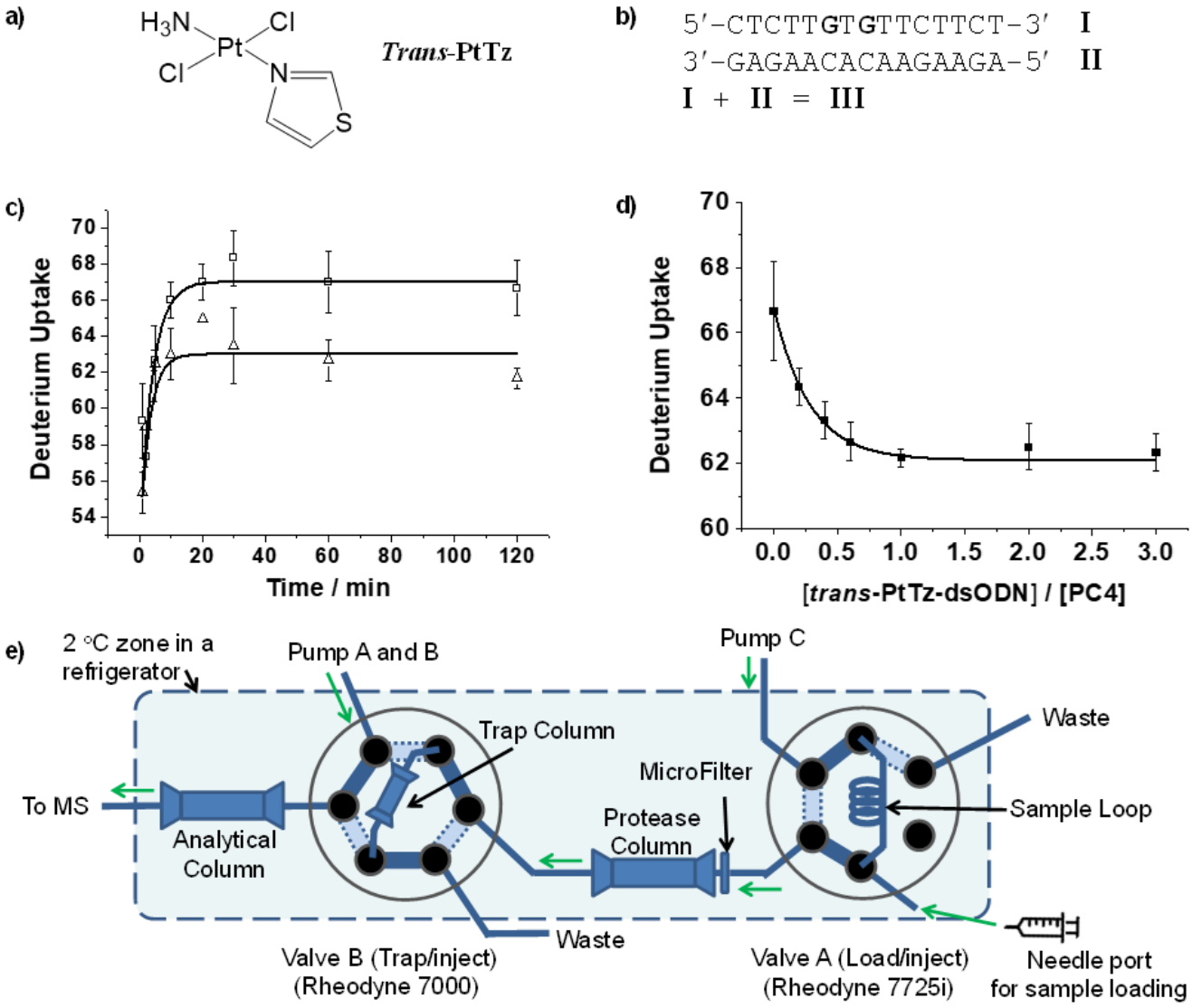


Figure 1

a, Chemical structure of *trans*-[$PtCl_2(NH_3)$(thiazole)] (*trans*-PtTz). **b**, the sequences of single strand ODN **I**, **II** and double stranded **III** used in this work. The guanine bases in bold in strand **I** refer to the 1,3-platination sites. **c**, Kinetic curves for the global deuterium uptake of native PC4 (square) and ligated PC4 with 1,3-*trans*-PtTz-**III** (triangle). **d**, The global deuterium uptake of PC4 as a function of molar ratio of 1,3-*trans*-PtTz-**III** to PC4. The hydrogen/deuterium exchange time was 60 min at 293 K, and the deuterium incorporation numbers are the means of three independent measurements. **e**, Schematic set up of the online digestion and peptide separation device in this work. Green arrows indicate the direction of samples and mobile phases. Valve A is in position “inject” (solid lines) and can be switched to “load” (dashed lines). Valve B is in position displayed in solid lines for sample loading in trap column and can be shifted to position in dashed lines for HPLC analysis.

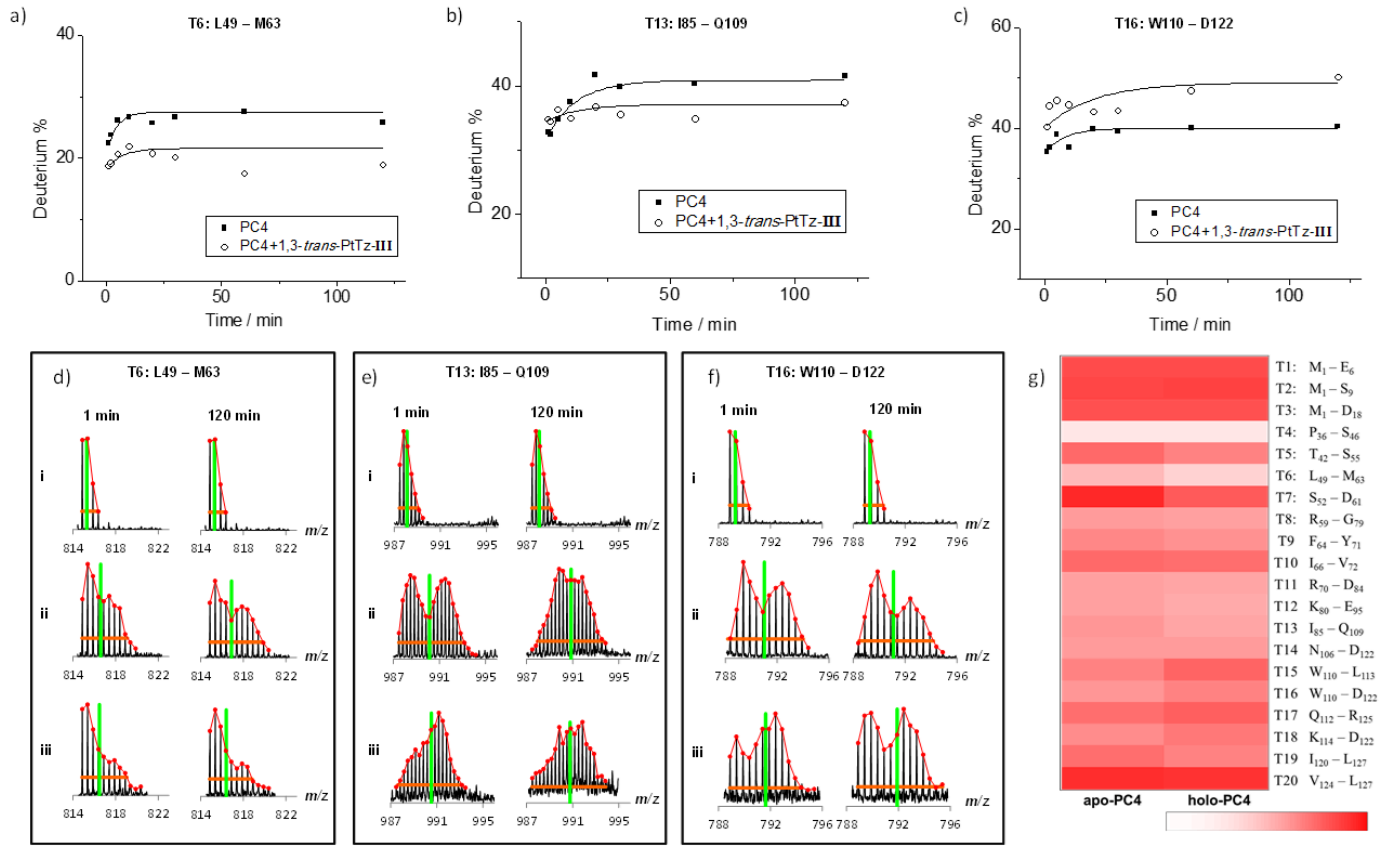


Figure 2

(**a, b, c**) Kinetic curves of HDX of peptic peptides T6, T13 and T16 arising from native PC4 (square) and ligated PC4 with 1,3-*trans*-PtTz-**III** (circle). (**d, e, f**) Mass spectra of non-deuterated (i) and deuterated (ii and iii) peptides T6, T13 and T16. The deuterated peptides derived from the native PC4 (ii) and the ligated PC4 with 1,3-*trans*-PtTz-**III** (iii) incubated in D_2O buffer for 1 min and 120 min, respectively. The vertical green line corresponds to the central *m/z* of each deuterated peptide. (**g**) Heat map for deuteration rate (relative to a fully exchanged control) of amides in peptic peptides derived from native (apo-PC4) and 1,3-*trans*-PtTz-**III** bound PC4 (holo-PC4) as assessed by HDX-MS. The relative deuteration rates were measured after 60 min of incubation of the protein in D_2O buffer and are assigned according to the color key shown in the bottom. Also see the location of each peptide in the protein in Supplementary Fig. S3.

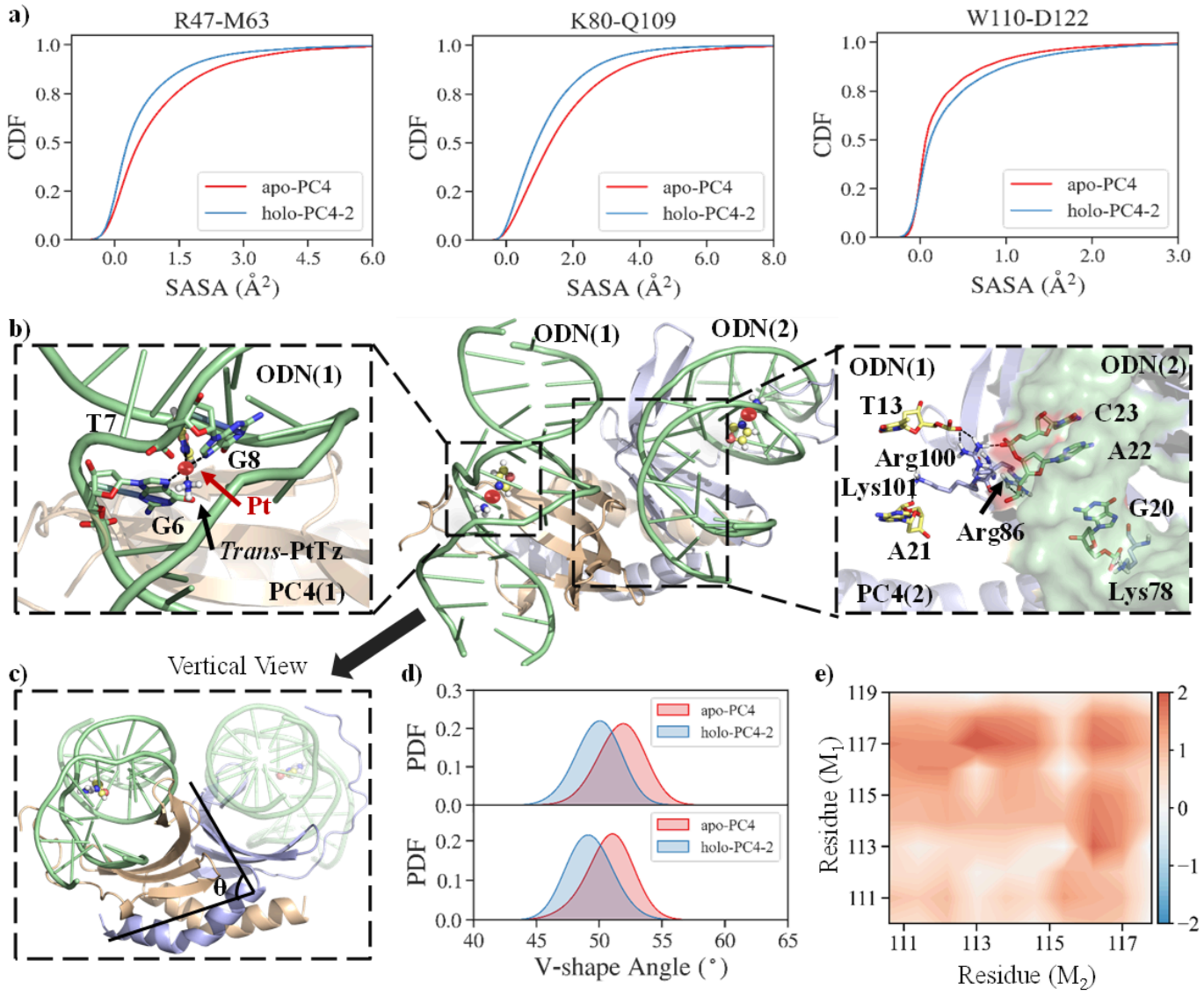


Figure 3

a, The cumulative distributions of SASA (solvent accessible surface area) of the apo-PC4 (red) and holo-PC4-2 (blue) of the R47-M63 (N-terminal disordered binding region), K80-Q109 (β-sheet binding region) and W110-D122 (C-terminal dimeric α-helices) segments; **b**, The representative structure, holo-PC4-2, of four holo-PC4 complexes. The monomer 1 and monomer 2 of PC4, and the two bound 1,3-*trans*-PtTz-**III** are shown in light yellow, light blue and pale green color, respectively. *Trans*-PtTz is shown in ball-and-stick model. The left panel is an enlarged view of the *trans*-PtTz binding region with ODN and the right panel shows an enlargement view of the key residues involved in the binding of PC4 to 1,3-*trans*-PtTz-III. Only one subunit of PC4 is shown for clarity. The corresponding nucleotides and amino acids are represented in a stick model. **c**, Schematic illustration of the V-shaped structure formed by the PC4 dimer. **d**, Probability density distribution of the V-shaped angle for apo-PC4 and holo-PC4-2. **e**, Matrix showing the closest distance differences between protein residues in apo-PC4 and holo-PC4-2 (calculated as holo-PC4-2 minus apo-PC4).

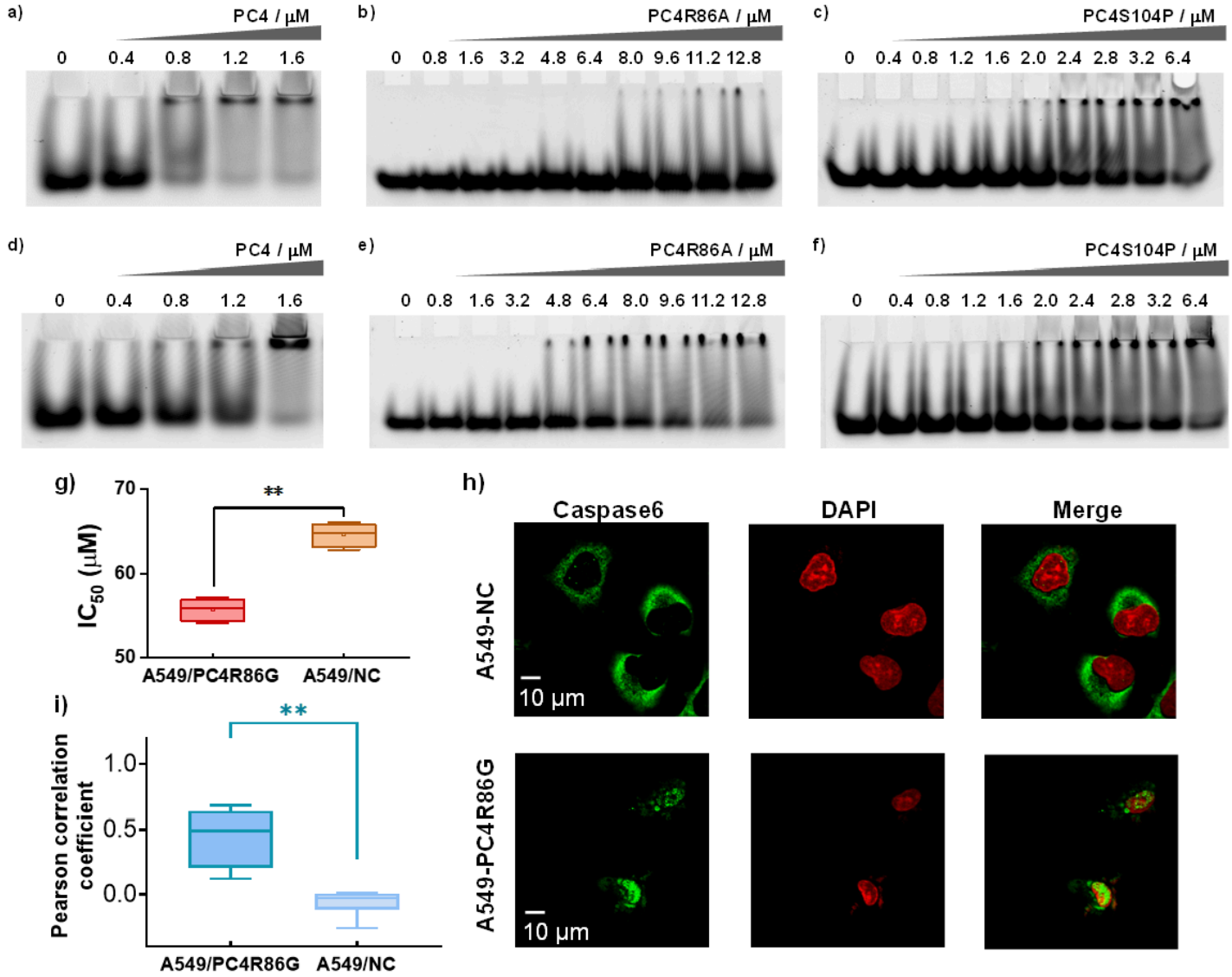


Figure 4

a – f, Electrophoretic mobility shift assays (EMSA) of double-stranded ODN duplex in the presence of various types of PC4 proteins. **a – c**, 1, 3-*trans*-PtTz-**III** (0.1 mM) and **d – f**, duplex **III** (0.1 mM) incubated with different concentrations of wild type PC4 (**a**, **d**), PC4R86A mutant (**b**, **e**) and PC4S104P mutant (**c**, **f**). **g – i**, The effect of the mutation of Arg86 to Gly on the sensitivity of A549 cells towards *trans*-PtTz. **g**, The IC_{50} values of *trans*-PtTz against A549/PC4R86G and A549/NC cells; **h**, Fluorescent images of A549/PC4R86G and A549/NC cells treated with 30 mM *trans*-PtTz for 24 h. Green represents the immunofluorescence signal of caspase6, red the fluorescence signal of cell nucleus stained by DAPI. **i**, Statistic chart of co-localization ratio (Pearson correlation coefficient) of caspase-6 with DAPI in A549/PC4R86G and A549/NC cells. ** indicates $p < 0.01$.

Supplementary Files

This is a list of supplementary files associated with this preprint. Click to download.

- SupplementaryMaterials20260109submit.docx